

Article

Preparation and Properties of Flexible CuI/Polyvinylpyrrolidone Nanocomposite Thermoelectric Film

Xiaowen Han, Xinru Zuo, Ying Liu, Zixing Wang and Kefeng Cai * 

Key Laboratory of Advanced Civil Engineering Materials of Ministry of Education, Shanghai Key Laboratory of Development and Application for Metal-Functional Materials, School of Materials Science & Engineering, Tongji University, Shanghai 201804, China; 18616350526@163.com (X.H.); 18295924921@163.com (X.Z.); liuying_polymer@163.com (Y.L.); wzxing2023@163.com (Z.W.)

* Correspondence: kfcai@tongji.edu.cn

Abstract: A facile preparation method for flexible p-type CuI/polyvinylpyrrolidone (PVP) nanocomposite thermoelectric (TE) film is developed. First, CuI powder was synthesized by a one-pot method; second, PVP was coated in situ with the CuI powder; third, the CuI/PVP nanocomposite film was prepared on a nylon membrane by vacuum filtration and then hot-pressing. Transmission electron microscopy (TEM) observation indicates that the film consists of CuI nanograins with an average size of ~15 nm and PVP distributed at the inner wall of nanopores and the surface of the CuI nanograins. The composite film shows a large Seebeck coefficient of ~605 μVK^{-1} and a power factor of ~8.05 $\mu\text{Wm}^{-1}\text{K}^{-2}$ at 300 K. The nanocomposite film also exhibits excellent flexibility (~96% of initial electrical conductivity retention after being bent 1000 times along a 4 mm radius rod). A single-leg TE module outputs a voltage of ~3.6 mV when the temperature difference is 6 K. This work provides a fast, simple, and environmentally friendly method by which to prepare flexible CuI/PVP nanocomposite TE film with a large Seebeck coefficient, which could be used as a wearable sensor.

Keywords: thermoelectric; CuI; PVP; nanocomposite; flexibility



Citation: Han, X.; Zuo, X.; Liu, Y.; Wang, Z.; Cai, K. Preparation and Properties of Flexible CuI/Polyvinylpyrrolidone Nanocomposite Thermoelectric Film. *J. Compos. Sci.* **2023**, *7*, 461. <https://doi.org/10.3390/jcs7110461>

Academic Editor: Aleksey A. Vedyagin

Received: 13 September 2023

Revised: 18 October 2023

Accepted: 1 November 2023

Published: 3 November 2023



Copyright: © 2023 by the authors. Licensee MDPI, Basel, Switzerland. This article is an open access article distributed under the terms and conditions of the Creative Commons Attribution (CC BY) license (<https://creativecommons.org/licenses/by/4.0/>).

1. Introduction

Owing to the excessive pursuit of industrialization, the global energy crisis is becoming more and more serious, and the use of fossil fuels has also caused serious harm to the environment, such as global warming, acid rain, pollution of the soil environment, and animal extinction. Therefore, it is urgent to explore sustainable new energy to replace traditional fossil fuels [1,2]. Thermoelectric (TE) material is a kind of material with wide application prospects. It can convert heat energy into electrical energy directly by the transport of carriers within solids under a low-temperature difference [3]. The performance of TE materials is evaluated by a dimensionless figure of merit, $ZT = S^2\sigma T k^{-1}$, where S is the Seebeck coefficient, σ is the electrical conductivity, T is the absolute temperature, k is the total thermal conductivity, and $S^2\sigma$ is called the power factor (PF). A good TE material should have a high electrical conductivity, a large Seebeck coefficient, and a low thermal conductivity. However, these three parameters are strongly coupled to each other and hence it is a great challenge to obtain a high ZT value. Various approaches have been chosen to improve TE performance, such as doping, nanostructuring, annealing, alloying, and so on, and much progress has been made in several material systems [4], such as SnSe [5,6], Cu₂Se [7,8], and GeTe [9,10].

In recent years, the demand for wearable electronic devices has explosively increased. But most of the devices are powered by traditional batteries, which need to be replaced or recharged frequently. And this may limit further development of the wearable devices [11,12]. Recently, wearable sensors, which can be installed or worn on the human body to transmit, sense, and process information, have been widely used in consumer electronics, fitness, and health fields. The wearable sensors play an important role, especially

in healthcare and treatment. TE materials with good TE properties and flexibility have also attracted attention in the development of wearable sensors [13–16]. Therefore, more and more researchers pay attention to flexible TE materials [17,18].

At present, there are three typical types of high-performance flexible TE material. The first one uses organic polymers, usually conductive polymers, such as poly(3,4-ethylenedioxythiophene)/poly(styrenesulfonate) (PEDOT: PSS), polypyrrole (PPy), polyaniline (PANI), and so on [19–22]. PEDOT: PSS, in which PSS is a styrene sulfonic acid group, is the most widely studied polymer. PEDOT: PSS exhibits p-type semiconductor characteristics. The electrical conductivity of PEDOT: PSS is between $\sim 10^{-4}$ and 10^3 Scm^{-1} [23,24]. By optimizing its composition and removing the PSS group, its PF can approach $\sim 500 \mu\text{Wcm}^{-1}\text{K}^{-2}$ and the ZT reaches ~ 0.42 [25]. These organic materials have good flexibility; however, their TE properties are much lower than those of traditional brittle inorganic TE materials. The second one involves exfoliation of the inorganic TE materials by a top-down method. For example, most recently, Lu et al. [26] demonstrated good pliability over 1000 bending cycles and high power factors of 4200 (p-type) and 4600 (n-type) $\mu\text{W m}^{-1}\text{K}^{-2}$ in Bi_2Te_3 -based films that were exfoliated from corresponding single crystals. This method can completely retain the excellent TE properties of inorganic materials; however, the process is costly and it is difficult to scale up production. The third one involves preparation of organic–inorganic composite TE materials, which have both good flexibility due to the organic component and high TE properties due to the inorganic component. Organic–inorganic composite TE materials can be divided into self-supporting films and flexible substrate-supported films. Generally, the composite films based on a flexible substrate show higher TE properties than the self-supporting films. A variety of methods can be used to prepare such films, such as vacuum filtration, screen printing, vapor deposition, rotary coating [27], electrochemical deposition, and magnetron sputtering [28–31], and there are many flexible substrates, such as polyimide (PI) membrane [32], nylon filter membrane, cellulose fiber, and even carbon paper. Huang et al. [28] prepared flexible Cu_2Se films by vapor deposition of Cu_2Se on a PI surface. The ratio of Cu and Se can be adjusted by controlling the thermal evaporation time. The maximum PF of $\text{Cu}_{2.09}\text{Se}$ film is $\sim 5.3 \mu\text{Wcm}^{-1}\text{K}^{-2}$ and the ZT is ~ 0.35 at room temperature. After bending 800 times at a bending radius of 6.5 mm, the electrical conductivity of the film remains 97% of the original. Jin et al. [33] deposited Bi_2Te_3 on cellulose fibers by magnetron sputtering to form a flexible composite film with a nano-micron-sized porous structure. The porous structure can introduce strong phonon scattering; hence, the thermal conductivity of the Bi_2Te_3 /cellulose fiber composite was significantly low. At 473 K, the ZT is ~ 0.38 . When the bending radius is 10 mm, the resistance increases to 1.05% after bending 100 times. However, as Se is scarce, and Te is toxic and expensive, it is very desirable to explore low-cost and environmentally friendly inorganic TE materials near room temperature.

CuI is a semiconductor with a wide direct band gap ($E_g = 3.1 \text{ eV}$) [34]. The reserves of iodine and copper are very abundant on the earth, and both of these components are non-toxic. It is noted that CuI is a green material [35,36]. In previous years, research on CuI has focused on optoelectronic and electronic applications [37–40]. CuI has three crystal structures which are closely related to the temperature. When the temperature is below 643 K, CuI shows the structure of sphalerite (γ phase); when the temperature is between 643 and 673 K, CuI shows the structure of wurtzite (β phase); when the temperature is above 673 K, it shows the structure of a plane cube (α phase). The α phase and β phase are both ionic conductors, while the γ phase at room temperature is a p-type semiconductor. The copper vacancy (V_{Cu}) has the lowest formation energy and ionization energy among all the native defects in either I-rich or Cu-rich growth conditions, and is primarily responsible for the p-type conductivity of CuI . Yadav et al. [34] calculated the TE properties of different phases of CuI based on the Boltzmann transport theory combined with first principles. It is found that the Seebeck coefficient of CuI increases monotonously with increasing temperature at low hole concentrations, which shows that there is no compensation between the hole and the electron. High Seebeck coefficient values have been found for all three

phases of CuI, and the typical Seebeck coefficient of γ -CuI at 300 K is $\sim 237 \mu\text{VK}^{-1}$ (at a hole concentration of 10^{20} cm^{-3}). Since then, the TE properties of CuI have attracted increasing attention, especially CuI films [41–43]. For example, Murmu et al. [43] deposited CuI films using an ion beam sputtering under a high vacuum at an ambient temperature and annealed the resulting CuI films in a quartz tube filled with argon. The electrical conductivity of the deposited CuI film is $\sim 21.9 \text{ Scm}^{-1}$ and the Seebeck coefficient is $\sim 264.7 \mu\text{VK}^{-1}$. After annealing at 250 °C, the electrical conductivity of the film decreased to 5.1 Scm^{-1} , which is 76% of that before annealing, while the Seebeck coefficient increased to $789.5 \mu\text{VK}^{-1}$, which is ~ 3 times as high as that before annealing, and the final PF was $740.9 \mu\text{Wm}^{-1}\text{K}^{-2}$. Optical transparency of the CuI film in the visible range is found to be 60–85%. However, the film is inflexible. CuI film has been deposited on polyethylene terephthalate (PET) substrate by magnetron sputtering [44], varying the iodine partial pressure in the sputter chamber during the magnetron sputtering to control the hole concentration of the CuI films. The obtained CuI film has a Seebeck coefficient of $\sim 172 \mu\text{VK}^{-1}$, a PF $\sim 359 \mu\text{Wm}^{-1}\text{K}^{-2}$, and $ZT \sim 0.21$ at room temperature, which is attributed to a combined effect of the heavy element iodine and strong phonon scattering. With a compressive bending angle up to 90°, the change in the internal resistance is $<3\%$, and, after repeatedly bending up to 400 cycles, the change in the internal resistance is $<0.2\%$. A prototype of a CuI-based transparent TE module shows good mechanical flexibility with a high power density of $\sim 2.4 \text{ mWcm}^{-2}$ at a temperature difference (ΔT) of 50 K, which shows the great potential of the CuI film as a transparent flexible TE material, and the power density of the CuI film is comparable with those of $\text{Bi}_2\text{Te}_3/\text{Sb}_2\text{Te}_3$ -based devices. Klochko et al. [45] synthesized CuI film on a nanocellulose (NC) substrate via a successive ionic layer adsorption and reaction (SILAR) method. The CuI/NC films obtained by repeating 25–40 SILAR cycles consist of cubic (111)-oriented γ -CuI crystals with faceted surfaces of 200–300 nm. The CuI/NC films have a PF of $\sim 140 \mu\text{Wm}^{-1}\text{K}^{-2}$ at 333 K. When the temperature difference is 40 K, the CuI/NC-based single TE leg can generate a voltage of 3.5 mV and a maximum power of 3.8 nW. However, these methods, including pulsed laser deposition [43], sputtering [44,46], and SILAR [45,47], are expensive and time-consuming.

Our group recently developed a method for the synthesis of Ag_2Se nanowires combined with vacuum filtration and hot-pressing to prepare flexible Ag_2Se film on nylon. This Ag_2Se film has PF $\sim 987 \mu\text{Wm}^{-1}\text{K}^{-2}$ at room temperature, and it has good flexibility [48]. Based on this process, our group has successfully prepared various kinds of flexible Ag_2Se -based composite TE film [49–54], such as polyvinylpyrrolidone (PVP)/ Ag_2Se composite film, starting from Ag_2Se nanostructures coated with PVP, the PF of which can reach $\sim 1910 \mu\text{Wm}^{-1}\text{K}^{-2}$ (corresponding $ZT \sim 1.1$) at room temperature [49]. The PVP (molecular formula being $(\text{C}_6\text{H}_9\text{NO})_n$) acts as a great additive for improving flexibility (a 5.5% decrease in PF after being bent along a rod with a radius of 4 mm 1000 times) and the PVP-coated Ag_2Se nanostructures can disperse more evenly in ethanol leading to a more homogeneous film. This is because PVP is a non-ionic surfactant that has good solubility in water and most organic solvents and can well disperse inorganic nanoparticles due to forming a uniform PVP coating nanolayer on the nanoparticles. PVP has high solubility in both polar and non-polar solvents, biocompatibility, good complexation, good adhesion, low toxicity, and good spinnability [55]. Although PVP is insulating, which will have a negative effect on electrical conductivity, it also has extremely low thermal conductivity; if only a very small amount of PVP is added, the direct effect of adding PVP on the thermoelectric performance of the composite film could be neglected.

In our previous work [56], we reported the preparation and TE properties of CuI film, but the film was porous and hence with ultralow electrical conductivity and low stability. Hence, in this work, PVP is used to improve the flexibility, electrical conductivity, and stability of the CuI film. PVP-coated CuI powder was prepared in situ by a one-pot method at room temperature, and then flexible CuI/PVP film was prepared on a nylon membrane combined with vacuum filtration and hot-pressing. The TE properties and flexibility of

the CuI/PVP nanocomposite films were investigated. In addition, a flexible single-leg TE module was fabricated with the nanocomposite film, and its touch tests were investigated.

2. Materials and Methods

All the raw materials, including copper nitrate trihydrate ($\text{Cu}(\text{NO}_3)_2 \cdot 3\text{H}_2\text{O}$), potassium iodide (KI), polyethylene glycol (PEG), polyvinylpyrrolidone (PVP), hydrazine hydrate ($\text{N}_2\text{H}_4 \cdot \text{H}_2\text{O}$), and ethanol, were purchased from sinopharm Chemical Reagent Co., Ltd., Shanghai, China.

In a typical procedure, PVP-coated CuI powder was prepared as follows: first, 1.3288 g of $\text{Cu}(\text{NO}_3)_2 \cdot 3\text{H}_2\text{O}$ and 2 g of PEG were dissolved in 50 mL ethanol to form solution A and 0.83 g of KI and 2 g of PEG were dissolved in 50 mL ethanol to form solution B. Second, a certain amount of PVP (0.01 g, 0.03 g or 0.05 g) and 100 μL $\text{N}_2\text{H}_4 \cdot \text{H}_2\text{O}$ were added to solution B with stirring. Third, solution B was slowly added into solution A with continuous stirring for 20 min. Finally, PVP-coated CuI powder was collected by centrifugation and washed with ethanol and deionized water (DI) several times.

The PVP-coated CuI powder was ultrasonically dispersed in ethanol for 5 min, and then deposited on a porous nylon membrane via vacuum-assisted filtration. The as-prepared film was dried in a vacuum oven for 24 h at 65 °C then hot-pressed at 230 °C and 1 MPa for 30 min to obtain CuI/PVP composite film. Figure 1 shows a schematic diagram of the preparation of the CuI/PVP composite film. Schematic illustration of CuI grain growth with PVP when hot-pressing is illustrated in Figure S8. To study the effect of the content of PVP on CuI, PVP content was adjusted from 0.01 and 0.03 to 0.05 g; for simplicity, the corresponding powders were named P1-powder, P2-powder, and P3-powder, respectively, and the corresponding films were named P1-film, P2-film, and P3-film, respectively. Pure CuI powder and film were named P0-powder and P0-film, respectively.

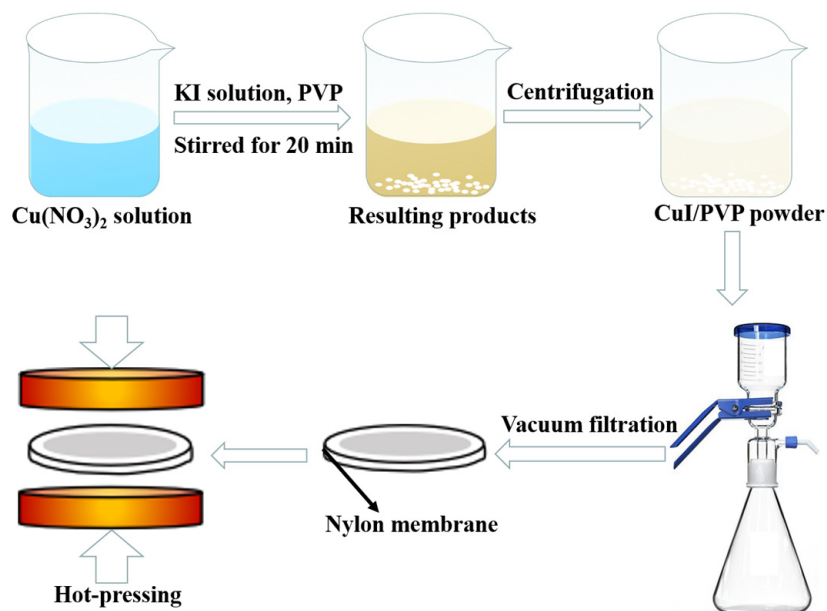


Figure 1. Schematic diagram of the preparation process of CuI/PVP composite film.

A flexible single-leg TE module was fabricated by first sticking a strip (20 mm \times 5 mm) of the CuI/PVP composite film onto polyimide (PI) substrate with a double-faced adhesive tape; then, Ag paste (SPI# 04998-AB) was painted onto two ends of the strip to connect with conducting wires. A finger touch test on a single-leg TE module was tested by a self-made experimental instrument (see Figure S8). As Figure S8 shows, in the single-leg TE module, heat transfers from the hot side to the cold side along the length direction of the module. We used an automatic temperature controlling system to heat a copper plate and one end of the module was put on the plate as the hot side ($T + \Delta T$). The other end of the module

was put in the air as the cold side (T). Then, we collected the output voltage at a particular temperature difference.

The electrical conductivity at room temperature was measured using a four-probe technical machine, with the help of a Hall effect measurement system (Ecopia HMS-3000). The Seebeck coefficient at room temperature was measured by the slope of the linear relationship between the thermal electromotive force and temperature difference (ΔT) between two ends on one side of each film. The temperature-dependent TE properties were measured by a Cryoall CTA-3 instrument in He atmosphere, with an instrument test error of $\pm 5\%$ for both electrical conductivity and Seebeck coefficient. The flexibility of composite film was tested by measuring the electrical conductivity after bending the film along a rod with a radius of 4 mm at different times.

The crystallinity and phase composition of the CuI powder and films were examined by X-ray diffraction (XRD) (Bruker D8 Advance). All XRD measurements were recorded in the 2θ range of $10\text{--}90^\circ$ at a scanning speed of $5^\circ/\text{min}$. The thickness of the film was around $10.87\ \mu\text{m}$, which was determined by field-emission scanning electron microscopy (FESEM, FEI Nova NanoSEM 450) observation of the cross-section of the film. The FESEM observation was also used to examine the surface morphology of CuI powder and CuI/PVP films. High-resolution transmission electron microscopy (HRTEM) (JEM-2100F) was used to observe the CuI powder. A transmission electron microscope (TEM, Titan Themis G2 60-300, Thermo Fisher Scientific, Shanghai, China) was used to investigate the internal details of the film.

3. Results

X-ray diffraction (XRD) patterns of the P1-film and P1-powder are shown in Figure 2a. As seen, all peaks are indexed to the γ -CuI with no impurity peaks [57]. The CuI thin film exhibits strong peaks at (111), (220), and (311) planes. Note that the (220) and (311) peaks of the P1-film are stronger than those of P1-powder, showing that hot-pressing improves the crystallinity of the CuI. No XRD peaks of PVP are detected, which may be because of its small content and amorphous characteristic [49]. Figure 2b and Figure S1a show scanning electron microscopy (SEM) images of P1 and P0-powder. From the SEM images, P0-powder consists of numerous nanoparticles and thin slices, and P1-powder is composed of many slices with an average size of $\sim 1\ \mu\text{m}$. It was noticed that adding PVP changes the morphology of the CuI powder. Figure 2c shows a TEM image of the P1-powder. There is an amorphous layer with an average thickness of $\sim 20\ \text{nm}$ uniformly coated on the surface of the CuI powder. Considering that a small content of PVP is added in situ when synthesizing CuI and that no impurity peaks (Figure 2a) are detected, we think that the amorphous layer is PVP. Figure 2d and Figure S1c show typical surface SEM images of the P1-film and the CuI film reported in our previous work [56]. By comparing Figure 2d with Figure S1c, the P1-film is denser. This is probably because the PVP-coated CuI powder can disperse more evenly in ethanol to avoid agglomeration, forming a more uniform film after vacuum filtration. Figure 2e is a cross-sectional SEM image of the P1-film, which also shows that the film is dense with a small amount of nanopores.

Figure 3 shows TEM and high-resolution TEM (HRTEM) images of the P1-film. The P1-film consists of nanograins with an average size of $\sim 15\ \text{nm}$. Figure 3b is an enlarged image of the red box in (a), and Figure 3c is an enlarged image of the green box in (a). Figure 3b,c shows that CuI nanograins are connected by an amorphous PVP phase and there exists a small number of nanopores ($\sim 5\text{--}10\ \text{nm}$). The insets of Figure 3c show inverse fast Fourier transform (IFFT) images corresponding to grains A and C. Notably, the crystallinity of the CuI grains is good. Figure 3d displays an HRTEM image of another area, which shows several connected grains coated with an amorphous PVP layer. Figure 3e shows a semi-coherent GB. The insets of Figure 3e show the corresponding IFFT and fast Fourier transform (FFT) images, indicating that the lattice spacings of regions A and B are both $0.349\ \text{nm}$, corresponding to the (111) plane of CuI. Figure 3f displays a twin boundary, which can significantly reduce the thermal conductivity and has little effect on the electrical

conductivity [58]. Figure 3g shows an HRTEM image containing several grains. Figure 3h,i shows enlarged images of the orange and blue boxes marked in (g). Figure 3h shows a typical triangular GB, indicating the three grains (grains A, B, and C) are well-sintered together. Figure 3i displays grains A, B, and another grain (grain D). It is deduced from the different contrasts of the grains (Figure S6) that grain D lies beneath grains A and B. Namely, in the P1-film, most CuI grains are sintered, and a small number of CuI grains are bonded by PVP.

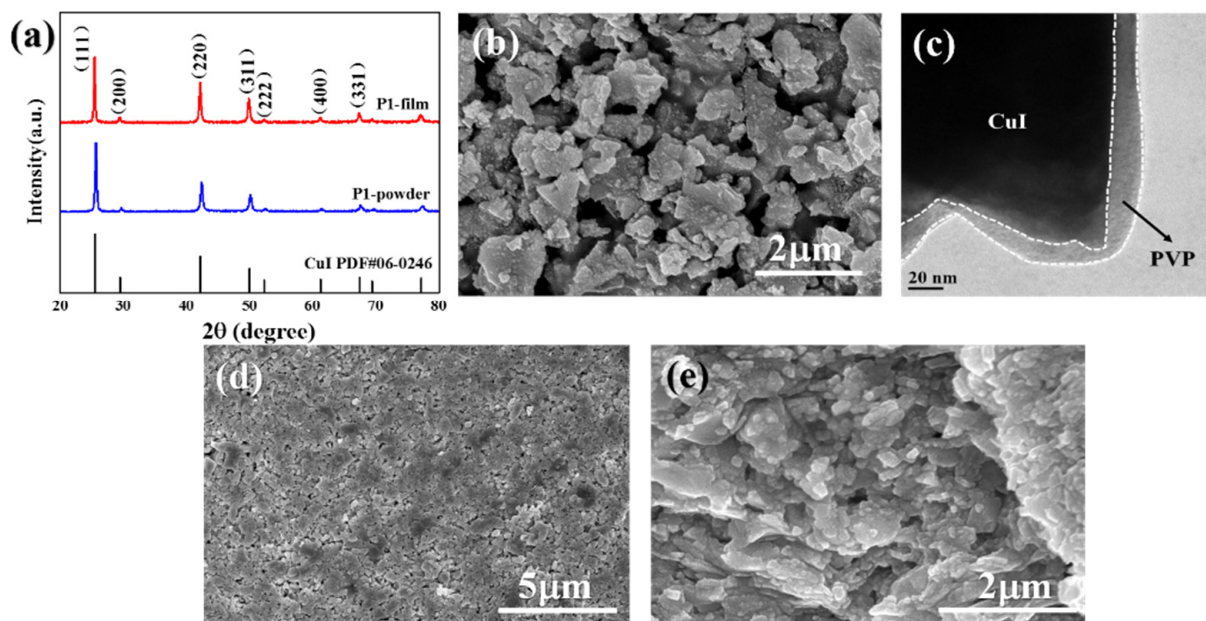


Figure 2. (a) XRD pattern of P1-powder and P1-film; (b) SEM image of P1-powder; (c) TEM image of P1-powder; (d) a typical SEM image of P1-film; (e) cross-sectional SEM image of P1-film.

The TE performances of P0-film, P1-film, P2-film, and P3-film at room temperature are shown in Table 1. It can be seen from Table 1 that, with increasing PVP content, the Seebeck coefficient increases from 522 to 605 μVK^{-1} and then gradually decreases, which indicates that the films are p-type conductors. The variation in electrical conductivity is consistent with the variation of the Seebeck coefficient, which may be related to the content of PVP. Compared with the P0-film, the electrical conductivity and Seebeck coefficient of the P1-film are larger. There are two opposing effects of adding PVP. One is that PVP is an insulating polymer, which leads to the degradation of the electrical conductivity of the composite film. The other is that adding PVP makes the composite film more uniform and denser, which is beneficial for increasing the electrical conductivity. For the P1-film, the amount of PVP added is very small and the latter effect of increasing electrical conductivity is more significant, but for the P2-film and P3-film, the amount of PVP added is more, and hence the former effect of decreasing electrical conductivity is more significant. However, the Seebeck coefficient is not sensitive to the density. Dun et al. [59] studied $\text{Cu}_{0.1}\text{Bi}_2\text{Se}_3$ nanoplatelet/polyvinylidene fluoride (PVDF) composite films. They think that there could be an energy filtration effect at the $\text{Cu}_{0.1}\text{Bi}_2\text{Se}_3$ /PVDF interface, leading to an increase in the Seebeck coefficient. However, because PVDF is an insulator, the energy barrier between PVDF and $\text{Cu}_{0.1}\text{Bi}_2\text{Se}_3$ could be so high that no carriers can surmount it. In the present case, PVP is also an insulator; hence, the reason for the P1-film having an enhanced Seebeck coefficient value is not clear yet. Consequently, P1-film exhibits an enhanced PF of $\sim 8.05 \mu\text{Wm}^{-1}\text{K}^{-2}$ at room temperature. Therefore, PVP should not be added too much in the synthesis process. In this work, the CuI/PVP mass ratio of $\sim 0.0095:1$ was the best, so P1-film was chosen for further study.

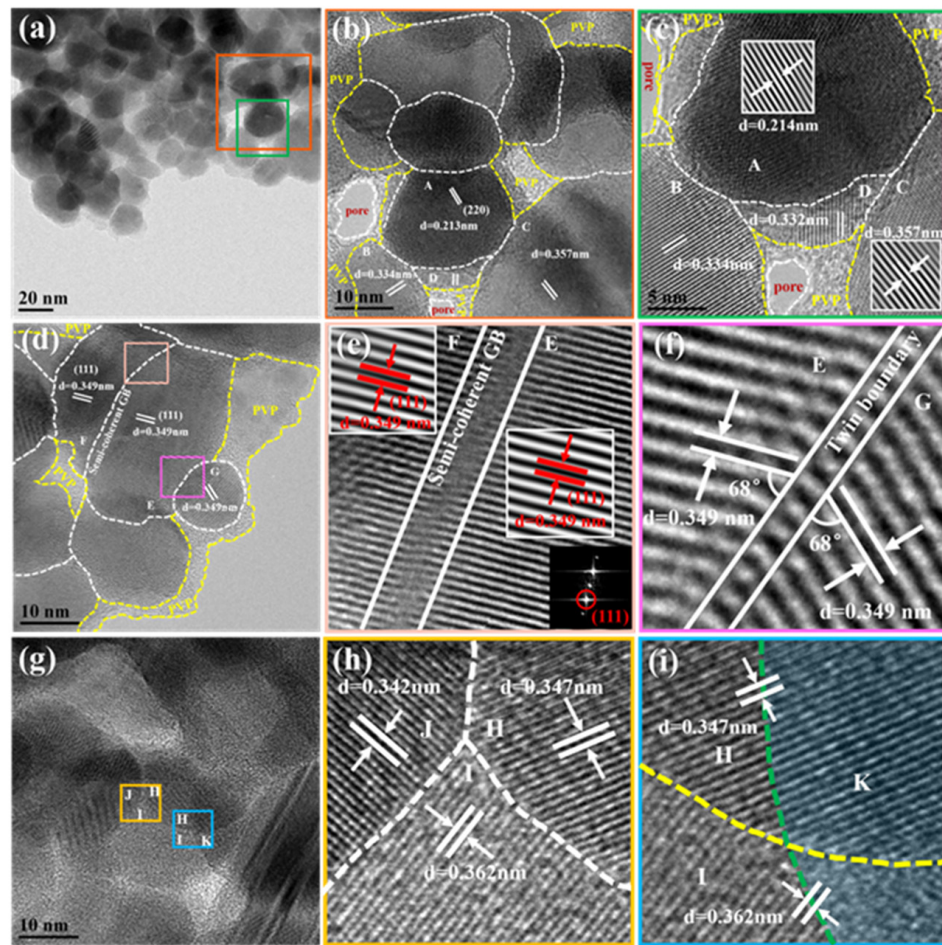


Figure 3. Microstructure characterization of the P1-film. (a) Overview TEM image of the P1-film; (b,c) enlarged images of the red and green box in (a), insets in (c) are the corresponding respective IFFT images; (d) A HRTEM image containing several connected grains; (e) enlarged image of the pink box in (d), insets are the corresponding IFFT and FFT images; (f) enlarged image of the purple box in (d); (g) an HRTEM image containing several grains; (h,i) enlarged images of the orange and blue boxes marked in (g), respectively. The uppercased letters in the figure such as A, B, C denote different grains.

Table 1. TE performances of the P0–P3 films at room temperature.

Sample	Mass Ratio (PVP:CuI)	S (μVK^{-1})	σ (Scm^{-1})	PF ($\mu\text{Wm}^{-1}\text{K}^{-2}$)
P0-film	0:1	522	0.18	4.94
P1-film	0.0095:1	605	0.22	8.05
P2-film	0.0286:1	374	0.17	2.38
P3-film	0.0477:1	332	0.14	1.54

Figure 4a shows the TE performance of the P1-film from 20 °C to 105 °C. Over the entire temperature range, the Seebeck coefficient value remains about $\sim 600 \mu\text{VK}^{-1}$ as the temperature increases. The electrical conductivity is $\sim 0.22 \text{ Scm}^{-1}$ at room temperature, and it tends to increase slightly before 90 °C and then drops gradually. Finally, the PF of the P1-film increases gradually with the temperature. At room temperature, P1-film exhibits a PF of $\sim 8.05 \mu\text{Wm}^{-1}\text{K}^{-2}$. The PF of the P1-film is relatively low; however, it is higher than that of a CuI/amorphous carbon composite pellet, which exhibits a PF of $\sim 7.5 \mu\text{Wm}^{-1}\text{K}^{-2}$ (corresponding electrical conductivity of $\sim 0.5 \text{ Scm}^{-1}$ and Seebeck coefficients of $\sim 390 \mu\text{VK}^{-1}$); the PF of the composite pellet markedly decreases to a range of 0.119

to $0.637 \mu\text{VK}^{-1}$ after a two- to twelve-cycle measurement from room temperature (RT) to 200°C [60], which is somewhat lower than that of CuI/bacterial cellulose nanofiber (BCNF) composite film with a PF of $\sim 24.6 \mu\text{Wm}^{-1}\text{K}^{-2}$ at RT [61] and $\text{Cu}_{1.75}\text{Te}$ /polyvinylidene fluoride (PVDF) composite film with a PF of $23 \mu\text{Wm}^{-1}\text{K}^{-2}$ at RT [62]. Nevertheless, the component Te of the latter is toxic and expensive.

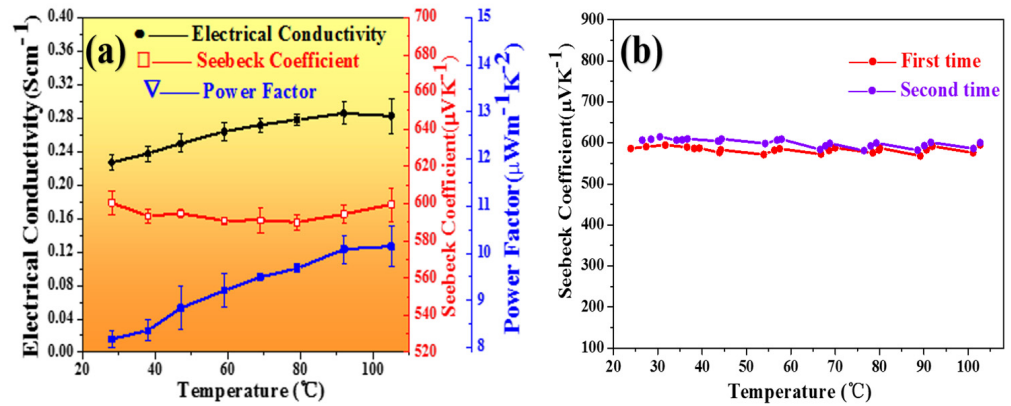


Figure 4. (a) Temperature–dependent Seebeck coefficient, electrical conductivity, and power factor of the P1–film; (b) temperature–dependent Seebeck coefficient of the P1–film for two heating cycles.

To study the thermal stability of P1-film, we tested temperature-dependent TE properties (the electrical conductivity and Seebeck coefficient) of the same film twice in succession, and the results are shown in Figures 4b and S4. Note that both parameters are almost the same during the two tests, suggesting that the prepared films have much better thermal stability below 100°C .

Figure 5a is a photo of the P1-film flexibility test. Figure 5b shows the flexibility test result. It indicates that, after being bent around a rod with a radius of 4 mm 1000 times, the electrical conductivity of P1-film decreases by only 4%, which is better than most of the reported flexible TE materials.

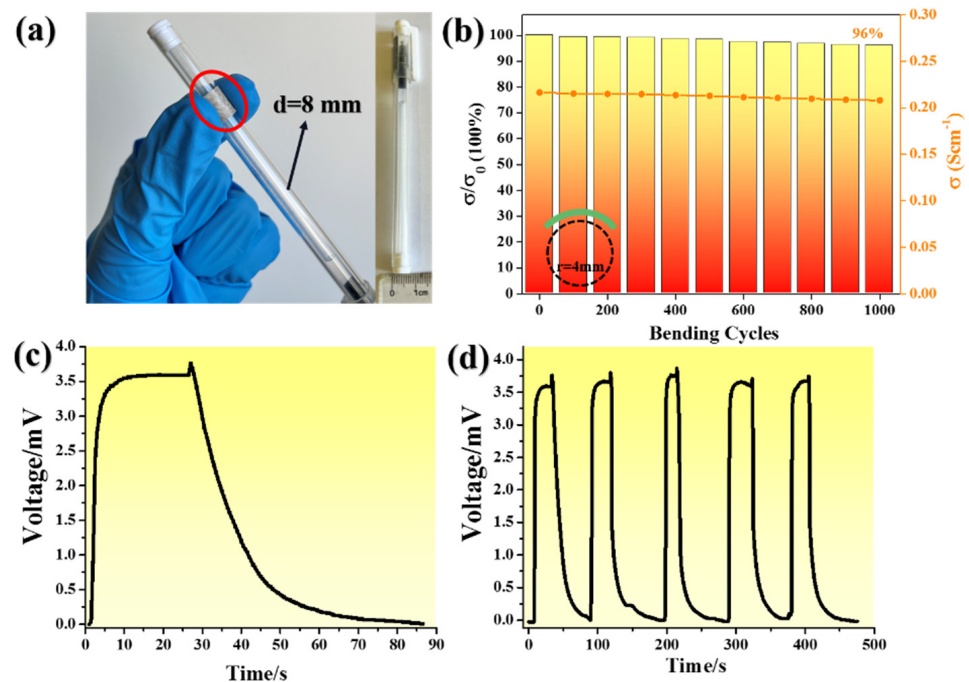


Figure 5. (a) Digital photo of P1–film flexibility test; (b) flexibility test result of the P1–film; the touch test for one–cycle (c), and five–cycle (d).

Compared with the CuI film reported in our previous work [56], the P1-film has better flexibility, higher electrical conductivity, and higher thermal stability, mainly because CuI nanograins in the film are sintered together and the adhesive effect of PVP.

Figure 5c,d shows the results of one-cycle and five-cycle touch tests on a single-leg TE module, respectively. In Figure 5c, note that when this module touched the heating plate, it immediately generated a voltage of ~1.5 mV in 0.5 s, reached a maximum voltage of about ~3.6 mV in 10 s and then remained the same voltage value. When moving this module away from the heating plate, the voltage quickly decreased to ~0 mV in ~60 s. Before moving the module from the heating plate, there was a slight increase in voltage, which may have been because the contact between the heating plate and the module enhanced somewhat before the module was moved away. It is indicated that the temperature difference (ΔT) between the heating plate and room temperature (29 °C) is 6 K. The Seebeck coefficient can be evaluated at about $\sim 600 \mu\text{VK}^{-1}$ using the formula $S = V/\Delta T$, which indicates the voltage touch test results are reliable. Figure 5d shows the result for multiple cycles. The peak voltage was somewhat different for each touch, which should be because the contact between the heating plate and the module was slightly different each time. The touch test shows that flexible PVP/CuI composite films have great potential prospects in wearable sensors.

4. Conclusions

In conclusion, we have prepared flexible CuI/PVP nanocomposite films by a simple method, and this method is environmentally friendly and highly efficient. In addition, PVP added in situ enhances the density and hence improves the flexibility, electrical conductivity and stability of the CuI film. TEM observation indicates that the film is composed of CuI nanograins (average size of ~15 nm) and PVP distributed at the surface of the CuI nanograins and the inner wall of nanopores. The optimized film shows a large Seebeck coefficient $\sim 605 \mu\text{VK}^{-1}$ and PF $\sim 8.05 \mu\text{Wm}^{-1}\text{K}^{-2}$ at room temperature, and the film exhibits excellent flexibility ($\sim 96\%$ of initial electrical conductivity retention after being bent 1000 times along a 4 mm radius rod). A single-leg TE module outputs a voltage of ~3.6 mV when ΔT is 6 K. This work provides a feasible and simple method for preparing dense and low-cost flexible TE nanocomposite films.

Supplementary Materials: The following supporting information can be downloaded at: <https://www.mdpi.com/article/10.3390/jcs7110461/s1>. Figure S1: SEM images of (a) P0-powder, (b) P3-film, and (c) CuI film for our previous work; Figure S2: Surface SEM images of (a) P1-film and (b) P3-film (CP); Figure S3: A typical cross-sectional SEM image of the P1-film; Figure S4: Temperature-dependent electrical conductivity of P1-film for two heating cycles; Figure S5: TEM images of P1 powder (a,b), (c) HRTEM image corresponding to the orange rectangle marked in (b); Figure S6: TEM images of P1 film; Figure S7: Schematic illustration of CuI grain growth and PVP behavior with hot-pressing; Figure S8: Schematic illustration of (a) a single-leg TE module and (b) a finger touch test on a single-leg TE module.

Author Contributions: X.H.: methodology, investigation, data curation, writing—original draft; X.Z.: formal analysis; Y.L.: visualization; Z.W.: formal analysis; K.C.: conceptualization, resources, writing—review and editing, supervision, funding acquisition. All authors have read and agreed to the published version of the manuscript.

Funding: This work was supported by the National Natural Science Foundation of China (Nos. 92163118, and 51972234).

Data Availability Statement: The data presented in this study are available in this article and supplementary material.

Conflicts of Interest: The authors declare no conflict of interest.

References

1. Höök, M.; Tang, X. Depletion of fossil fuels and anthropogenic climate change—A review. *Energy Policy* **2013**, *52*, 797–809. [[CrossRef](#)]
2. Leonov, V.; Vullers, R.J.M. Wearable electronics self-powered by using human body heat: The state of the art and the perspective. *J. Renew. Sustain. Energy* **2009**, *1*, 062701. [[CrossRef](#)]
3. Wang, L.; Zhang, Z.; Liu, Y.; Wang, B.; Fang, L.; Qiu, J.; Zhang, K.; Wang, S. Exceptional thermoelectric properties of flexible organic-inorganic hybrids with monodispersed and periodic nanophase. *Nat. Commun.* **2018**, *9*, 3817. [[CrossRef](#)]
4. Nandihalli, N.; Gregory, D.H.; Mori, T. Energy-Saving Pathways for Thermoelectric Nanomaterial Synthesis: Hydrothermal/Solvothermal, Microwave-Assisted, Solution-Based, and Powder Processing. *Adv. Sci.* **2022**, *9*, e2106052. [[CrossRef](#)] [[PubMed](#)]
5. Su, L.; Shi, H.; Wang, S.; Wang, D.; Qin, B.; Wang, Y.; Chang, C.; Zhao, L. Enhancing Carrier Mobility and Seebeck Coefficient by Modifying Scattering Factor. *Adv. Energy Mater.* **2023**, *13*, 2300312. [[CrossRef](#)]
6. Nguyen, V.Q.; Trinh, T.L.; Chang, C.; Zhao, L.-D.; Nguyen, T.H.; Duong, V.T.; Duong, A.T.; Park, J.H.; Park, S.; Kim, J.; et al. Unidentified major p-type source in SnSe: Multivacancies. *NPG Asia Mater.* **2022**, *14*, 42. [[CrossRef](#)]
7. Jin, Z.; Mao, T.; Qiu, P.; Yue, Z.; Wang, L.; Zhao, K.; Ren, D.; Shi, X.; Chen, L. Thermoelectric properties and service stability of Ag-containing Cu₂Se. *Mater. Today Phys.* **2021**, *21*, 100550. [[CrossRef](#)]
8. Li, M.; Cortie, D.L.; Liu, J.; Yu, D.; Islam, S.M.K.N.; Zhao, L.; Mitchell, D.R.; Mole, R.A.; Cortie, M.B.; Dou, S.; et al. Ultra-high thermoelectric performance in graphene incorporated Cu₂Se: Role of mismatching phonon modes. *Nano Energy* **2018**, *53*, 993–1002. [[CrossRef](#)]
9. Wang, C.; Wu, J.; Zeng, Z.; Embs, J.; Pei, Y.; Ma, J.; Chen, Y. Soft-mode dynamics in the ferroelectric phase transition of GeTe. *npj Comput. Mater.* **2021**, *7*, 118. [[CrossRef](#)]
10. Abdellaoui, L.; Chen, Z.; Yu, Y.; Luo, T.; Hanus, R.; Schwarz, T.; Villoro, R.B.; Cojocar-Mirédin, O.; Snyder, G.J.; Raabe, D.; et al. Parallel Dislocation Networks and Cottrell Atmospheres Reduce Thermal Conductivity of PbTe Thermoelectrics. *Adv. Funct. Mater.* **2021**, *31*, 2101214. [[CrossRef](#)]
11. Du, Y.; Shen, S.Z.; Cai, K.; Casey, P.S. Research progress on polymer-inorganic thermoelectric nanocomposite materials. *Prog. Polym. Sci.* **2012**, *37*, 820–841. [[CrossRef](#)]
12. Hewitt, C.A.; Kaiser, A.B.; Roth, S.; Craps, M.; Czerw, R.; Carroll, D.L. Multilayered carbon nanotube/polymer composite based thermoelectric fabrics. *Nano Lett.* **2012**, *12*, 1307–1310. [[CrossRef](#)] [[PubMed](#)]
13. Wang, Z.; Si, Y.; Zhao, C.; Yu, D.; Wang, W.; Sun, G. Flexible and Washable Poly(Ionic Liquid) Nanofibrous Membrane with Moisture Proof Pressure Sensing for Real-Life Wearable Electronics. *ACS Appl. Mater. Interfaces* **2019**, *11*, 27200–27209. [[CrossRef](#)] [[PubMed](#)]
14. Xia, S.; Wang, M.; Gao, G. Preparation and application of graphene-based wearable sensors. *Nano Res.* **2022**, *15*, 9850–9865. [[CrossRef](#)]
15. Li, Y.; Wang, S.; Xiao, Z.-C.; Yang, Y.; Deng, B.-W.; Yin, B.; Ke, K.; Yang, M.-B. Flexible TPU strain sensors with tunable sensitivity and stretchability by coupling AgNWs with rGO. *J. Mater. Chem. C* **2020**, *8*, 4040–4048. [[CrossRef](#)]
16. Nandihalli, N.; Liu, C.-J.; Mori, T. Polymer based thermoelectric nanocomposite materials and devices: Fabrication and characteristics. *Nano Energy* **2020**, *78*, 105186. [[CrossRef](#)]
17. Fan, Z.; Razavi, H.; Do, J.-W.; Moriwaki, A.; Ergen, O.; Chueh, Y.-L.; Leu, P.W.; Ho, J.C.; Takahashi, T.; Reichertz, L.A.; et al. Three-dimensional nanopillar-array photovoltaics on low-cost and flexible substrates. *Nat. Mater.* **2009**, *8*, 648–653. [[CrossRef](#)]
18. Zhao, W.; Liu, Z.; Sun, Z.; Zhang, Q.; Wei, P.; Mu, X.; Zhou, H.; Li, C.; Ma, S.; He, D.; et al. Superparamagnetic enhancement of thermoelectric performance. *Nature* **2017**, *549*, 247–251. [[CrossRef](#)]
19. Qu, S.; Yao, Q.; Wang, L.; Chen, Z.; Xu, K.; Zeng, H.; Shi, W.; Zhang, T.; Uher, C.; Chen, L. Highly anisotropic P3HT films with enhanced thermoelectric performance via organic small molecule epitaxy. *NPG Asia Mater.* **2016**, *8*, e292. [[CrossRef](#)]
20. Wang, J.; Cai, K.; Shen, S. A facile chemical reduction approach for effectively tuning thermoelectric properties of PEDOT films. *Org. Electron.* **2015**, *17*, 151–158. [[CrossRef](#)]
21. Wang, J.; Cai, K.; Song, H.; Shen, S. Simultaneously enhanced electrical conductivity and Seebeck coefficient in Poly (3,4-ethylenedioxythiophene) films treated with hydroiodic acid. *Synth. Met.* **2016**, *220*, 585–590. [[CrossRef](#)]
22. Ni, D.; Song, H.; Chen, Y.; Cai, K. Free-standing highly conducting PEDOT films for flexible thermoelectric generator. *Energy* **2019**, *170*, 53–61. [[CrossRef](#)]
23. Alamer, F.A.; Althagafy, K.; Alsalmi, O.; Aldeih, A.; Alotaiby, H.; Althabaiti, M.; Alghamdi, H.; Alotibi, N.; Saeedi, A.; Zabarmawi, Y.; et al. Review on PEDOT:PSS-Based Conductive Fabric. *ACS Omega* **2022**, *7*, 35371–35386. [[CrossRef](#)]
24. Shi, H.; Liu, C.; Jiang, Q.; Xu, J. Effective Approaches to Improve the Electrical Conductivity of PEDOT:PSS: A Review. *Adv. Electron. Mater.* **2015**, *1*, 1500017. [[CrossRef](#)]
25. Kim, G.-H.; Shao, L.; Zhang, K.; Pipe, K.P. Engineered doping of organic semiconductors for enhanced thermoelectric efficiency. *Nat. Mater.* **2013**, *12*, 719–723. [[CrossRef](#)]
26. Lu, Y.; Zhou, Y.; Wang, W.; Hu, M.; Huang, X.; Mao, D.; Huang, S.; Xie, L.; Lin, P.; Jiang, B.; et al. Staggered-layer-boosted flexible Bi₂Te₃ films with high thermoelectric performance. *Nat. Nanotechnol.* **2023**, 1–8. [[CrossRef](#)]

27. Kim, W.S.; Anoop, G.; Jeong, I.-S.; Lee, H.J.; Bin Kim, H.; Kim, S.H.; Goo, G.W.; Lee, H.; Lee, H.J.; Kim, C.; et al. Feasible tuning of barrier energy in PEDOT:PSS/Bi₂Te₃ nanowires-based thermoelectric nanocomposite thin films through polar solvent vapor annealing. *Nano Energy* **2020**, *67*, 104207. [[CrossRef](#)]
28. Huang, X.-L.; Ao, D.-W.; Chen, T.-B.; Chen, Y.-X.; Li, F.; Chen, S.; Liang, G.-X.; Zhang, X.-H.; Zheng, Z.-H.; Fan, P. High-performance copper selenide thermoelectric thin films for flexible thermoelectric application. *Mater. Today Energy* **2021**, *21*, 100743. [[CrossRef](#)]
29. Xie, J.; Han, M.; Zeng, X.; Mao, D.; Li, H.; Zeng, X.; Liu, R.; Ren, L.; Sun, R.; Xu, J. Flexible pCu₂Se-nAg₂Se thermoelectric devices via in situ conversion from printed Cu patterns. *Chem. Eng. J.* **2022**, *435*, 135172. [[CrossRef](#)]
30. Varghese, T.; Hollar, C.; Richardson, J.; Kempf, N.; Han, C.; Gamarachchi, P.; Estrada, D.; Mehta, R.J.; Zhang, Y. High-performance and flexible thermoelectric films by screen printing solution-processed nanoplate crystals. *Sci. Rep.* **2016**, *6*, 33135. [[CrossRef](#)]
31. Norimasa, O.; Chiba, T.; Hase, M.; Komori, T.; Takashiri, M. Improvement of thermoelectric properties of flexible Bi₂Te₃ thin films in bent states during sputtering deposition and post-thermal annealing. *J. Alloys Compd.* **2022**, *898*, 162889. [[CrossRef](#)]
32. Goo, G.; Anoop, G.; Unithrattil, S.; Kim, W.S.; Lee, H.J.; Kim, H.B.; Jung, M.-H.; Park, J.; Ko, H.C.; Jo, J.Y. Proton-Irradiation Effects on the Thermoelectric Properties of Flexible Bi₂Te₃/PEDOT:PSS Composite Films. *Adv. Electron. Mater.* **2019**, *5*, 1800786. [[CrossRef](#)]
33. Jin, Q.; Shi, W.; Zhao, Y.; Qiao, J.; Qiu, J.; Sun, C.; Lei, H.; Tai, K.; Jiang, X. Cellulose Fiber-Based Hierarchical Porous Bismuth Telluride for High-Performance Flexible and Tailorable Thermoelectrics. *ACS Appl. Mater. Interfaces* **2018**, *10*, 1743–1751. [[CrossRef](#)] [[PubMed](#)]
34. Yadav, M.K.; Sanyal, B. First-principles study of thermoelectric properties of CuI. *Mater. Res. Express* **2014**, *1*, 15708. [[CrossRef](#)]
35. Thomas, S.; Hildreth, O.; Zaeem, M.A. Unveiling the effect of vacancy defects on structural, mechanical, electronic and diffusion properties of copper (I) iodide. *Scr. Mater.* **2022**, *213*, 114634. [[CrossRef](#)]
36. Xu, Z.L.; Yang, C.; Wu, Y.N. Temperature-dependent electronic structure of gamma-phase CuI: First-principles insights. *J. Phys. Condens. Matter* **2022**, *34*, 134002.
37. Yuan, P.; Chen, R.; Zhang, X.; Chen, F.; Yan, J.; Sun, C.; Ou, D.; Peng, J.; Lin, S.; Zheng, N.; et al. Ether-Soluble Cu₅₃ Nanoclusters as an Effective Precursor of High-Quality CuI Films for Optoelectronic Applications. *Angew. Chem. Int. Ed. Engl.* **2019**, *58*, 835–839. [[CrossRef](#)] [[PubMed](#)]
38. Seifert, M.; Kawashima, M.; Rödl, C.; Botti, S. Layered CuI: A path to 2D p-type transparent conducting materials. *J. Mater. Chem. C* **2021**, *9*, 11284–11291. [[CrossRef](#)]
39. Huang, Y.; Tan, J.; Gao, G.; Xu, J.; Zhao, L.; Zhou, W.; Wang, Q.; Yuan, S.; Sun, J. Transparent p-type CuI film based self-powered ultraviolet photodetectors with ultrahigh speed, responsivity and detectivity. *J. Mater. Chem. C* **2022**, *10*, 13040–13046. [[CrossRef](#)]
40. Cha, J.-H.; Jung, D.-Y. Air-Stable Transparent Silver Iodide-Copper Iodide Heterojunction Diode. *ACS Appl. Mater. Interfaces* **2017**, *9*, 43807–43813. [[CrossRef](#)]
41. Kneiß, M.; Yang, C.; Barzola-Quiquia, J.; Benndorf, G.; von Wenckstern, H.; Esquinazi, P.; Lorenz, M.; Grundmann, M. Suppression of Grain Boundary Scattering in Multifunctional p-Type Transparent γ -CuI Thin Films due to Interface Tunneling Currents. *Adv. Mater. Interfaces* **2018**, *5*, 1701411. [[CrossRef](#)]
42. Mulla, R.; Rabinal, M.K. Defect-Controlled Copper Iodide: A Promising and Ecofriendly Thermoelectric Material. *Energy Technol.* **2018**, *6*, 1178–1185. [[CrossRef](#)]
43. Murmu, P.P.; Karthik, V.; Liu, Z.; Jovic, V.; Mori, T.; Yang, W.L.; Smith, K.E.; Kennedy, J.V. Influence of Carrier Density and Energy Barrier Scattering on a High Seebeck Coefficient and Power Factor in Transparent Thermoelectric Copper Iodide. *ACS Appl. Energy Mater.* **2020**, *3*, 10037–10044. [[CrossRef](#)]
44. Yang, C.; Souchay, D.; Kneiß, M.; Bogner, M.; Wei, H.M.; Lorenz, M.; Oeckler, O.; Benstetter, G.; Fu, Y.Q.; Grundmann, M. Transparent flexible thermoelectric material based on non-toxic earth-abundant p-type copper iodide thin film. *Nat. Commun.* **2017**, *8*, 16076. [[CrossRef](#)] [[PubMed](#)]
45. Klochko, N.; Barbash, V.; Klepikova, K.; Kopach, V.; Tyukhov, I.; Yashchenko, O.; Zhadan, D.; Petrushenko, S.; Dukarov, S.; Sukhov, V.; et al. Efficient biodegradable flexible hydrophobic thermoelectric material based on biomass-derived nanocellulose film and copper iodide thin nanostructured layer. *Sol. Energy* **2020**, *212*, 231–240. [[CrossRef](#)]
46. Coroa, J.; Faustino, B.M.M.; Marques, A.; Bianchi, C.; Koskinen, T.; Juntunen, T.; Tittonen, I.; Ferreira, I. Highly transparent copper iodide thin film thermoelectric generator on a flexible substrate. *RSC Adv.* **2019**, *9*, 35384–35391. [[CrossRef](#)]
47. Klochko, N.; Zhadan, D.; Klepikova, K.; Petrushenko, S.; Kopach, V.; Khrypunov, G.; Lyubov, V.; Dukarov, S.; Khrypunova, A. Semi-transparent copper iodide thin films on flexible substrates as p-type thermolegs for a wearable thermoelectric generator. *Thin Solid Films* **2019**, *683*, 34–41. [[CrossRef](#)]
48. Ding, Y.; Qiu, Y.; Cai, K.; Yao, Q.; Chen, S.; Chen, L.; He, J. High performance n-type Ag₂Se film on nylon membrane for flexible thermoelectric power generator. *Nat. Commun.* **2019**, *10*, 841. [[CrossRef](#)]
49. Jiang, C.; Wei, P.; Ding, Y.; Cai, K.; Tong, L.; Gao, Q.; Lu, Y.; Zhao, W.; Chen, S. Ultrahigh performance polyvinylpyrrolidone/Ag₂Se composite thermoelectric film for flexible energy harvesting. *Nano Energy* **2021**, *80*, 105488. [[CrossRef](#)]
50. Li, Y.; Lou, Q.; Yang, J.; Cai, K.; Liu, Y.; Lu, Y.; Qiu, Y.; Lu, Y.; Wang, Z.; Wu, M.; et al. Exceptionally High Power Factor Ag₂Se/Se/Polypyrrole Composite Films for Flexible Thermoelectric Generators. *Adv. Funct. Mater.* **2021**, *32*, 2106902. [[CrossRef](#)]
51. Li, X.; Lu, Y.; Cai, K.; Gao, M.; Li, Y.; Wang, Z.; Wu, M.; Wei, P.; Zhao, W.; Du, Y.; et al. Exceptional power factor of flexible Ag/Ag₂Se thermoelectric composite films. *Chem. Eng. J.* **2022**, *434*, 134739. [[CrossRef](#)]

52. Wu, M.; Cai, K.; Li, X.; Li, Y.; Liu, Y.; Lu, Y.; Wang, Z.; Zhao, W.; Wei, P. Ultraflexible and High-Thermoelectric-Performance Sulfur-Doped Ag₂Se Film on Nylon for Power Generators. *ACS Appl. Mater. Interfaces* **2022**, *14*, 4307–4315. [[CrossRef](#)] [[PubMed](#)]
53. Liu, Y.; Lu, Y.; Wang, Z.; Li, J.; Wei, P.; Zhao, W.; Chen, L.; Cai, K. High performance Ag₂Se films by a one-pot method for a flexible thermoelectric generator. *J. Mater. Chem. A* **2022**, *10*, 25644–25651. [[CrossRef](#)]
54. Jiang, C.; Ding, Y.; Cai, K.; Tong, L.; Lu, Y.; Zhao, W.; Wei, P. Ultrahigh Performance of n-Type Ag₂Se Films for Flexible Thermoelectric Power Generators. *ACS Appl. Mater. Interfaces* **2020**, *12*, 9646–9655. [[CrossRef](#)]
55. Khan, W.S.; Hamadneh, N.N.; Khan, W.A. Prediction of thermal conductivity of polyvinylpyrrolidone (PVP) electrospun nanocomposite fibers using artificial neural network and prey-predator algorithm. *PLoS ONE* **2017**, *12*, e0183920. [[CrossRef](#)] [[PubMed](#)]
56. Han, X.; Lu, Y.; Liu, Y.; Wu, M.; Li, Y.; Wang, Z.; Cai, K. CuI/Nylon Membrane Hybrid Film with Large Seebeck Effect. *Chin. Phys. Lett.* **2021**, *38*, 126701. [[CrossRef](#)]
57. Grundmann, M.; Schein, F.L.; Lorenz, M.; Böntgen, T.; Lenzner, J.; von Wenckstern, H. Cuprous iodide—A p-type transparent semiconductor: History and novel applications. *Phys. Status Solidi A* **2013**, *210*, 1671–1703. [[CrossRef](#)]
58. Zhang, A.; Zhang, B.; Lu, W.; Xie, D.; Ou, H.; Han, X.; Dai, J.; Lu, X.; Han, G.; Wang, G.; et al. Twin Engineering in Solution-Synthesized Nonstoichiometric Cu₅FeS₄ Icosahedral Nanoparticles for Enhanced Thermoelectric Performance. *Adv. Funct. Mater.* **2018**, *28*, 1705117. [[CrossRef](#)]
59. Dun, C.; Hewitt, C.A.; Huang, H.; Xu, J.; Zhou, C.; Huang, W.; Cui, Y.; Zhou, W.; Jiang, Q.; Carroll, D.L. Flexible n-type thermoelectric films based on Cu-doped Bi₂Se₃ nanoplate and Polyvinylidene Fluoride composite with decoupled Seebeck coefficient and electrical conductivity. *Nano Energy* **2015**, *18*, 306–314. [[CrossRef](#)]
60. Bai, S.-Q.; Wong, I.H.K.; Lin, M.; Young, D.J.; Hor, T.S.A. A thermoelectric copper-iodide composite from the pyrolysis of a well-defined coordination polymer. *Dalton Trans.* **2018**, *47*, 5564–5569. [[CrossRef](#)]
61. Li, H.; Zong, Y.; Li, X.; Ding, Q.; Jiang, Y.; Han, W. Biodegradable CuI/BCNF composite thermoelectric film for wearable energy harvesting. *Cellulose* **2021**, *28*, 10707–10714. [[CrossRef](#)]
62. Zhou, C.; Dun, C.; Wang, Q.; Wang, K.; Shi, Z.; Carroll, D.L.; Liu, G.; Qiao, G. Nanowires as Building Blocks to Fabricate Flexible Thermoelectric Fabric: The Case of Copper Telluride Nanowires. *ACS Appl. Mater. Interfaces* **2015**, *7*, 21015–21020. [[CrossRef](#)] [[PubMed](#)]

Disclaimer/Publisher's Note: The statements, opinions and data contained in all publications are solely those of the individual author(s) and contributor(s) and not of MDPI and/or the editor(s). MDPI and/or the editor(s) disclaim responsibility for any injury to people or property resulting from any ideas, methods, instructions or products referred to in the content.